Identification of Residues of the IFNAR1 Chain of the Type I Human Interferon Receptor Critical for Ligand Binding and Biological Activity†

Chantal Cajean-Feroldi,‡ Florence Nosal,§ Pierre C. Nardeux,‡ Xavier Gallet,§ Jacqueline Guymarho,‡ Florence Baychelier,‡ Pascal Sempé,§ Michael G. Tovey,‡ Jean-Louis Escary,§ and Pierre Eid*,‡

Laboratory of Viral Oncology, CNRS-UPR 9045, 7 rue Guy Moquet, 94801 Villejuif, France, and GenOdyssee S.A., 3 Avenue du Canada, BP 810 Les Ulis, 91974 Courtabœuf cedex, France

Received May 3, 2004; Revised Manuscript Received July 16, 2004

ABSTRACT: The antiviral and antiproliferative activities of human type I interferons (IFNs) are mediated by two transmembrane receptor subunits, IFNAR1 and IFNAR2. To elucidate the role of IFNAR1 in IFN binding and the establishment of biological activity, specific residues of IFNAR1 were mutated. Residues ^{62}FSSLKLNVY^{70} of the S5−S6 loop of the N-terminal subdomain of IFNAR1 and tryptophan-129 of the second subdomain of IFNAR1 were shown to be crucial for IFN-α binding and signaling and establishment of biological activity. Mutagenesis of peptide ^{278}LRV in the third subdomain shows that these residues are critical for IFN-α-induced biological activity but not for ligand binding. These data, together with the sequence homology of IFNAR1 with cytokine receptors of known structure and the recently resolved NMR structure of IFNAR2, led to the establishment of a three-dimensional model of the human IFN-α/IFNAR1/IFNAR2 complex. This model predicts that following binding of IFN to IFNAR1 and IFNAR2 the receptor complex assumes a "closed form", in which the N-terminal domain of IFNAR1 acts as a lid, resulting in the activation of intracellular kinases. Differences in the primary sequence of individual IFN-α subtypes and resulting differences in binding affinity, duration of ligand/receptor association, or both would explain differences in intracellular signal intensities and biological activity observed for individual IFN-α subtypes.

The human type I interferon (IFN) family is composed of 14 structurally related IFN-α subtypes and single IFN-*β* and IFN-*ω* subtypes. They adopt a five helix bundle fold, and all bind to a common transmembrane receptor composed of two polypeptide chains, IFNAR1 and IFNAR2. Although the NMR structure of the extracellular domain of IFNAR2 has recently been resolved (*1*), the specificities of the IFNAR1−ligand interactions remain largely unknown.

Alignment of the primary amino acid sequences of IFNAR1 and IFNAR2 with the sequences of other receptors led to their classification as members of the helical cytokine class II family of receptors (hCRII; *2*), which currently contains at least 12 members (*3*, *4*). IFNAR1 is the only member of this receptor superfamily with an extracellular domain composed of four fibronectin type III (FNIII) subdomains of approximately 100 amino acids each (denoted for simplicity SD1−SD4), which are in turn organized into two domains of 200 amino acids each, both of which appear to be required for establishment of the biological response to type I IFNs (*5*, *6*).

Binding of interferons to their cell surface receptor represents the initial and probably most specific step in the IFN signaling pathway. IFNAR1 and IFNAR2 cooperate to form a high-affinity receptor for all type I IFNs (*7*, *8*). It has been shown recently that a soluble form of the extracellular domain of huIFNAR2 retains the ability to bind IFN-α2 or IFN-*β* with a 1:1 stoichiometry (*9*, *10*). Despite the fact that IFNAR2 contributes more strongly than IFNAR1 to the binding of human type I IFNs, both subunits are required for high-affinity binding, maintenance of species specificity, and signal transduction (*11*, *12*).

Signal transduction is initiated after the initial binding of IFN to IFNAR1 and IFNAR2 (*7*, *8*, *13*, *14*) and formation of a ternary productive complex. IFN binding leads to activation of the tyrosine kinases Tyk2 and JAK1, which phosphorylate specific tyrosine residues on the signal transducers and activators of transcription STAT1 and STAT2, which then form a heterodimer that binds to IRF-9 to form the IFN-stimulated gene factor 3 (ISGF3) transcription factor complex. This complex then translocates to the nucleus leading to the activation of the transcription of those genes that contain an IFN-sensitive response element (ISRE) within their promoter region (*15*, *16*).

Identification of the residues critical for the productive contact of IFN with its receptor would contribute to our understanding of the mechanisms leading to activation of IFN-induced antiviral and antiproliferative activity. In the absence of the resolved crystal structure of the IFN−receptor complex or any experimentally determined 3-D structure for the IFN/IFNAR1 complex, a number of models for the extra-

† This work was supported in part by the Association Nouvelles Recherches Biomedicales, Pharma Pacific Pty, and Medarex Inc.

* Corresponding author. Phone: 33-1 49 58 34 37. Fax: 33-1 49 58 34 44. E-mail: eid@infobiogen.fr.

‡ CNRS-UPR 9045.

§ GenOdyssee S.A.

10.1021/bi049111r CCC: $27.50
Published on Web 09/11/2004

cellular domains of IFNAR1 and IFNAR2 (*17*−*19*) have been formulated on the basis of sequence homology with cytokine receptors of known structure. Recent NMR studies of the extracellular domain of IFNAR2 and its complex with IFN-α2 have identified the structural constraints of IFN binding to this receptor component resulting in the first determination of the structure of an interferon receptor chain in solution (*1*, *20*).

Site-directed mutagenesis of IFNAR2 (*19*, *21*) and IFN-α (*9*, *22*−*25*) and specific monoclonal antibodies to IFNAR1 and IFNAR2 (*18*, *26*−*28*) have also been used to map ligand−receptor binding sites and to study the structure−function relationships of the type I IFN receptor.

Uzé et al. (*22*) suggested on the basis of data obtained from experiments using a series of IFN-α hybrids that amino acid clusters on helix A and C bind the IFNAR1 subunit, leaving the AB loop, helix D, and the DE loop on the opposite face of the molecule free to interact with IFNAR2. Lewerenz et al. (*19*) identified groups of residues within loops S3−S4 and S5−S6 of the SD1 subdomain of IFNAR2 specifically involved in IFN-α binding. Subsequently, Runkel et al. (*29*) suggested the existence of binding sites for IFNAR1 and IFNAR2 on opposite faces of the IFN-β molecule. Piehler et al. (*24*) mapped the complete binding region of IFN-α2 on IFNAR2 by alanine scanning mutations showing that (1) helix E (in particular, residues R144, A145, M148, and R149) is located in the center of the binding site, flanked by residues in helix A and the AB loop (L30, R33) and (2) the contribution of helix D in the interaction is minor.

In contrast to the interaction of human IFN-α2 with IFNAR2, little is known about the binding of IFN-α2 to the IFNAR1 chain. This is due mainly to the low binding affinity of human IFNAR1. The high affinity of human IFN-α for the bovine IFNAR1 chain has permitted critical aromatic residues in bovine IFNAR1 responsible for human IFN-α binding to be identified by site-directed mutagenesis (*18*). Other studies using neutralizing monoclonal antibodies against IFNAR1 capable of blocking IFN-α binding and biological activity led to the identification of residues critical for antibody binding: the ^{71}EEIKLR^{76} strand in SD1 and the ^{246}HLYKWK^{251} loop and the ^{293}EEIKFDTE^{300} strand in SD3 (*26*). As shown previously (*27*), the ^{62}FSSLKLNVY^{70} peptide in SD1 is recognized by the 64G12 monoclonal antibody and most likely overlaps a binding site for both IFN-α and IFN-β. Kumaran et al. (*30*) have reported that the SD1 subdomain of IFNAR1 does not contribute to the species specificity that is associated with IFNAR1. In contrast, in this study, we demonstrate using site-directed mutagenesis that residues of the S5−S6 loop in the SD1 subdomain of human IFNAR1, together with a residue in the SD2 subdomain, are crucial for IFN-α binding and receptor function, while residues (^{278}LRV) in the SD3 subdomain were critical for IFN-α-induced biological activity but not for ligand binding.

We present herein a 3-D model of the IFN-α/IFNAR1/IFNAR2 complex based on biochemical data and knowledge of the structure of other receptors, which predicts a dynamic mechanism for interferon receptor complex activation. Thus, binding of different IFN-α subtypes would result in the formation of closed forms of the receptor in which the N-terminal SD1 subdomain of IFNAR1 would have a dynamic role acting as a lid, which folds over the bound IFN molecule.

EXPERIMENTAL PROCEDURES

Interferons and Antibodies. Recombinant human IFN-α2b with a specific activity of 2×10^8 IU/mg was purchased from Schering-Plough S.A., recombinant human IFN-α8 (2×10^8 IU/mg) was a gift from CIBA-Geigy (Basel, Switzerland), and recombinant human IFN "consensus" (IFN-cons) was provided by Dr. Janneke de Wal, Yamanouchi EU B.V. The 64G12 mAb, a mouse IgG1 that inhibits both the binding and biological activities of all the human type I IFNs tested, was prepared by immunizing mice with a recombinant protein corresponding to the extracellular domain of the IFNAR1 chain of the human IFN-α/β receptor expressed in mammalian cells as described previously (*31*). The anti-IFNAR1 mAbs (64G12 and 34F10) used in this study are species-specific and do not cross-react with IFNAR1 from mouse or bovine cell extracts as shown previously (*27*). Anti-IFNAR2 antibodies were obtained from Calbiochem, and the mouse monoclonal antibody (8F11) was raised against a recombinant form of the extracellular domain of human IFNAR2 (Eid, P., unpublished data). Rabbit anti-phospho-STAT1 was obtained from New England Biolabs, Beverly, MA, and anti-STAT2 and anti-phospho-STAT2 were obtained from Upstate Biotechnology, Charlottesville, VA.

Cell Culture. L-929 murine cells were cultivated in Dulbecco's modified Eagle's medium with Glutamax (DMEM, Life Technologies, Inc., Gaithersburg, MD). Human Burkitt lymphoma Daudi cells were grown in suspension culture in RPMI 1640 medium (Life Technologies, Inc, Gaithersburg, MD) at 37 °C in 5% CO_2. Cell cultures were supplemented with 10% heat-inactivated fetal bovine serum (HyClone), 10 units/mL penicillin, and 10 μg/mL streptomycin (Life Technologies, Inc., Gaithersburg, MD).

Parental Plasmids and Mutagenesis. Human IFNAR2 was expressed from the pEFIRESneo vector derived from pIRESneo2 (Clontech, Palo Alto, CA) in which the CMV promoter was replaced by the human EF-1α promoter from pDEF3 (a gift from J. Langer, New Jersey). Wild-type huIFNAR1 and all other mutants were expressed from pEFIREShyg derived from pIREShyg (Clontech, Palo Alto, CA) as described above. Mutagenesis of the IFNAR1 receptor chain was performed using the QuickChange site-directed mutagenesis kit (Stratagene, Amsterdam). Plasmids from each bacterial colony were screened by restriction enzyme digestion and the accuracy of all cDNA was confirmed by DNA sequencing.

DNA Transfection. As a first step, murine L929 cells, were stably transfected with vectors containing the wild-type human IFNAR2 receptor chain using FuGENE-6, according to the manufacturer's instructions (Roche, Basel, Switzerland). Transfected cells were selected in culture medium supplemented with 1.5 mg/mL G418 sulfate (Clontech, Palo Alto, CA). Transfectants expressing human IFNAR2 were selected by fluorescence activated cell sorter (FACS) analysis using anti-IFNAR2 mAbs.

In a second step, LR2 (wild-type human IFNAR2 transfectants) were stably transfected with vectors containing wild-type or mutated human IFNAR1 using the same procedure

as described for IFNAR2 except that the selection medium was supplemented with 1.5 mg/mL G418 sulfate and 400 μg/mL hygromycin B (Euromedex, France). Transfectants expressing human IFNAR1 receptors were selected after FACS analysis with anti-IFNAR1 mAbs and denominated WT, SK, VY, W, mutI, mutII, mutIII, or mutIV.

Radiolabeling of Interferon α-2 and Interferon α-"Consensus". Recombinant IFN-α2 or IFN-cons were radioiodinated as described previously (*32*) to a specific activity of 5×10^4 Bq/pmol. Each batch of radiolabeled IFN used in this study was tested for its ability to bind to human Daudi cells prior to use.

Binding Experiments with ^{125}I-Labeled Interferon. Binding experiments were performed on 1×10^6 cells harvested at 70−80% confluence after detaching adherent cells from the surface of plastic culture flasks with Accutase (PAA). The cells were incubated at 4 °C for 1.5 h in 500 μL of DMEM with 1% fetal bovine serum (FBS) with gentle shaking in the presence of various concentrations of labeled ligand (0.2−1 nM). Nonspecific binding was determined by measuring the binding of labeled ligand in the presence of a 100 fold molar excess of unlabeled interferon. The binding reaction was stopped by applying each fraction to 750 μL of frozen sucrose (10% in PBS). Cell pellets were separated by centrifugation (13 000 × *g*, 1 min), and cell associated radioactivity was counted in a γ counter (LKB, Upsala, Sweden).

Analysis of Cell Surface Receptor Expression. Binding studies were carried out on transfectants expressing levels of human IFNAR2 in excess of that of IFNAR1 using subnanomolar concentrations of human IFN under conditions where the IFNAR2 subunit was undersaturated. Thus, binding of human IFN to its receptor was determined from data obtained for total binding minus the binding due to IFNAR2 alone (LR2) according to the equation of Klotz and Hunston (*33*):

$$B = (K_{d_1}F/(1 + K_{d_1}F)) + (K_{d_2}F/(1 + K_{d_2}F))$$

where B represents the bound fraction, F represents the concentration of free ligand, and K_{d_1} and K_{d_2} represent the IFN receptor and IFNAR2 dissociation constants, respectively.

The apparent binding constant, K_d, and number of binding sites per cell were then determined, when possible, from the slope and intercept of the Scatchard's plot, respectively. To facilitate comparison of binding curves, ligand binding data was expressed as the "occupied site ratio", which represents the amount of bound ligand, normalized with respect to the number of binding sites at saturation of the double transfectant expressing both IFNAR1 and IFNAR2, after subtraction of ligand binding to IFNAR2 alone.

Flow-Cytometry Analysis of Cell Surface Receptor Expression Using Fluorescent Labeled Anti-IFNAR Antibodies. The number of binding sites per cell for LR2 and mutants VY and W was estimated from the mean relative fluorescence obtained using anti-IFNAR2 and anti-IFNAR1 mAbs by reference to the number of receptor sites per cell determined by Scatchard's analysis for WT, SK, and mutIV. Two millions cells were detached with Accutase (PAA Laboratories, Gmbh, Austria) and incubated with anti-IFNAR1 (64G12 or 34F10) or anti-IFNAR2 monoclonal antibodies (Abs) for 2 h at 4 °C. Primary Abs were detected using goat anti-mouse IgG conjugated to R-Phycoerythrin (Sigma) (40 min at 4 °C) followed by analysis on a FACSCalibur flow cytometer (Becton-Dickinson, Franklin Lakes, NJ). Data were acquired and analyzed using CELLQuest version 3.1 software (Becton-Dickinson, Franklin Lakes, NJ).

Cell Lysis and Immunoblotting of Phosphorylated Proteins. Cell lysis, immunoprecipitations, and immunoblotting were performed as described previously (*27*) with the following modifications. Proteins were fractionated on 8% sodium dodecyl sulfate−polyacrylamide gel electrophoresis (SDS−PAGE) under reducing conditions, transferred to poly(vinylidene difluoride) filters (PVDF, Boehringer Mannheim, Germany), and probed with the appropriate primary specific antibodies for 1 h at 20 °C, followed by the addition of a 1/100 000 dilution of the secondary antibody (horseradish peroxidase (HRP)-conjugated goat antimouse or antirabbit IgG, JACKSON Immunoresearch, Baltimore, MD) for 45 min at 20 °C. PVDF blots were developed using the SuperSignal WestPico kit (Pierce, Rockford, IL).

Electrophoretic Mobility-Shift Assays (EMSA). EMSA analysis was carried out as described previously (*26*). Cells were detached using Accutase and incubated with or without 2000 IU/mL of IFN-α2 or IFN-α8 for 30 min at 37 °C. The nuclear fraction was purified and cleared by centrifugation, and the supernatant was stored at −70 °C until use. An IFN-stimulated response element (ISRE) double-stranded ^{32}P-labeled probe (top, 5′-GAT CGG GAA AGG GAA ACC GAA ACT GAA GCC-3′; bottom, 5′-GAT CGG CTT CAG TTT CGG TTT CCC TTT CCC-3′; specific activity of 20×10^6 cpm/μg) was prepared from the ISG15 promoter. Three micrograms of nuclear extract, 60 000 cpm of labeled probe, and 4 μg of double-stranded nonspecific competitor poly(dI)−poly(dC) (Amersham Biosciences, U.K.) in 30 μL of binding buffer were used for binding reactions of extracts of IFN-treated or untreated cells. DNA−protein complexes were resolved on a 6% nondenaturing polyacrylamide gel (Sigma) and analyzed by autoradiography. The specificity of the assay was determined by the addition of 700 ng of unlabeled ISRE probe in a separate reaction mixture.

Antiviral Assays. For the determination of antiviral activity, cells were seeded at 75 000 cells/mL in a 24 well plate, incubated at 37 °C, and 24 h later treated with 10 IU/mL of IFN-α2, IFN-α8, or buffer alone. After a further 24 h incubation at 37 °C, the medium was discarded, and vesicular stomatitis virus (VSV) was added to the cells at a multiplicity of infection of 0.1 particles/cell in DMEM medium supplemented with 2% FBS (DMEM-2) for 1 h at 37 °C. The cells were then washed with DMEM-2 and resuspended in 1 mL of DMEM-2 per well and incubated at 37 °C for 24 h. After three consecutive freeze−thawing cycles at −80 °C, the supernatant containing VSV was centrifuged (10 000 × *g* for 10 min to remove cell debris), and the supernatant was titrated on murine L929 cells. Virus titers were expressed as tissue culture infectious dose ($TCID_{50}$) per 1 mL.

Cell Proliferation Assay. Cell proliferation was assessed using a FACSCalibur flow cytometer. Control and single and doubly transfected cells were seeded in 24 well plates at 20 000 cells per well in the presence of IFN-α2 or IFN-α8 (2000 IU/mL). Cells were counted at 24, 48, 72, and 96 h, and the cell number was compared to untreated cells. Briefly, cells were detached by trypsine/EDTA, recovered with 1 mL

of DMEM supplemented with 2% FCS, and fixed with 10% formaldehyde. An equal known number of calibrated beads was added to each sample, and the mixture was analyzed by FACS. Beads and cells appeared at well distinguished coordinates on a SSC/FSC plot. Cell number was proportional to the number of beads counted.

Construction of the IFNα-2/IFN Receptor Complex Model. The model of the IFNAR1 extracellular domain was constructed using the MODELER program (*34*) from the InsightII software (Accelrys, San Diego, CA). Its protein sequence (Figure 1) was divided into two parts (SD1−SD2 and SD3−SD4). Each part includes two FNIII domains. Both 3-D models were constructed by homology using the interferon γ receptor 1 (PDB entry 1fyh, subunit E; *35*) and the tissue factor receptor (TFR) (PDB entry 2hft; *36*) as templates. Multiple alignments were carried out with ClustalW. They yielded 18% and 15.5% sequence similarity for SD1−SD2 and SD3−SD4, respectively. Due to low sequence homology, both multiple alignments were refined using hydrophobic cluster analysis (*37*), which has been shown to be particularly efficient and sensitive with families of sequences sharing low levels of identity. A 3-D model of IFN-α8 was also constructed using the MODELER program and the structure of IFN-α2 as a template. For all MODELER runs, five models were built with the high-optimization protocol. The quality of all 3-D models was checked with the Profile-3D (*38*) and Verify programs as implemented in Insight II. The structure of the extracellular domain of IFNAR2 (PDB entry 1nv6; *1*) and the structure of IFN-α2 (PDB entry 1itf, *39*) determined by NMR spectroscopy were used for the construction of the IFN-α2/IFN receptor complex.

To obtain a better orientation of lateral chains in interfaces, the entire IFN-α2/IFNAR1/IFNAR2 complex was subjected to molecular mechanic calculations using the DISCOVER program (Accelrys, San Diego, CA) with the cff91 force field. The nonbond cutoff method and the dielectric constant, respectively, were set up as cell multipole- and distance-dependent. Initially, energy minimization was performed using a steepest descent algorithm, followed by a conjugated gradient algorithm (until the maximum derivative was less than 0.01 kcal/(mol Å)), whereas the Cα trace was tethered with a quadratic potential (for all secondary structures) and using distance constraints to maintain five interactions between IFNAR2 and IFN-α2 as described by Roisman et al. (*21*). These are 6 ± 1.5 Å between Phe27 (IFN-α2) and Tyr44 (IFNAR2), 3.5 ± 1 Å between Asp35 (IFN-α2) and Lys49 (IFNAR2), 4.5 ± 1 Å between R149 (IFN-α2) and E78 (IFNAR2), and 3.5 ± 1 Å between Ser152 (IFN-α2) and His77 (IFNAR2). A larger distance constraint (10 ± 1.5 Å) was assigned to the Arg144 (IFN-α2)/M47 (IFNAR2) pair due to the orientation of the arginine side chain toward the protein core in the structure of IFN-α2.

Calculation of Electrostatic Surfaces. The solvent-accessible surface of each model was displayed using the Connolly algorithm from InsightII with a solvent probe radius of 1.4 Å. Electrostatic potentials for IFN-α2, IFN-α8, and IFN-β and for the whole extracellular subdomains of IFNAR1 and IFNAR2 taken individually were computed using the DELPHI module of InsightII. A full Coulombic boundary condition was used with the dielectric constants set at 2 for the protein and 80 for the solvent. A map of 65 points × 65 points × 65 points was used with a grid fill of 80% for all IFN molecules and receptor subdomains, giving a grid step of 0.97 Å/point. The surface was colored red for potentials less than −3 kT (acidic), blue for potentials greater than +3 kT (basic), and white for neutral potentials of 0 kT. Colors between these values were produced using a linear interpolation.

RESULTS

Mutation of the Extracellular Domain of Human IFNAR1. The residues mutated in the first subdomain (SD1) of IFNAR1 were chosen on the basis of the previously determined location of the epitope recognized by the monoclonal antibody 64G12, which inhibits the binding and biological activity of all human type I interferons tested (*31*). This peptide ^{62}FSSLKLNVY^{70} mapped to a site within the S5−S6 loop of the SD1 subdomain, predicted by homology with other cytokine receptors, to be an exposed region potentially accessible to ligand binding (*40*). Two peptides (^{63}SSLK^{66}) and (^{69}VY), designated SK and VY, respectively, were substituted with alanine (Figure 1) to disrupt the heart of the epitope recognized by the 64G12 antibody. A group of four amino acids was replaced with alanine residues in the SK mutant. Residue Y70 has been shown to be absolutely necessary for the binding of the anti-IFNAR1 mAb to IFNAR1. Thus, its substitution inhibited binding of the mAb to the mutated peptide as demonstrated by Western blot analysis using total cell extracts from mutant VY (data not shown) and by ELISA using the mutated peptide as the target as described previously (*27*).

Tryptophan 129 was mutated to alanine in mutW based on the data reported by Cutrone et al. showing a 95% inhibition of IFN binding when the corresponding W132 (situated within 9−17 Å from the 64G12 epitope) of the bovine IFNAR1 homologue was mutated to alanine (*18*).

The four remaining mutants (mutI, mutII, mutIII, and mutIV) were generated in the SD2 and SD3 subdomains of IFNAR1 (Figure 1). The residues mutated in mutI (^{166}SPE) are located between the S5 and S6 strands in the SD2 subdomain of IFNAR1 distant from the IFN-α binding site, near the hinge region between subdomains SD2 and SD3. It was reasoned that mutation of these residues may shed light on the relative orientation of these subdomains.

Aromatic interactions are known to be important in the formation of cytokine receptor complexes. Despite the fact that tryptophan 183 or phenylalanine 271 are unlikely to be involved in IFN binding, mutants mutII (^{183}WKI) and mutIII (^{269}NVF) were designed to validate their orientation in the receptor complex.

Arginine 279 of the sequence ^{278}LRV of mutIV is located in the interface between the SD2 and SD3 subdomains of IFNAR1 and residue R279 and residue K240 constitute a major cluster responsible for the positive electrostatic potential on the surface of the SD3 subdomain. Facing this patch is a negative electrostatic potential cluster formed by the ^{109}EAED^{112} peptide on the surface of the SD2 subdomain.

Effect of Mutations SK and VY on the Ability of the Neutralizing Anti-Human IFNAR1 Monoclonal Antibody 64G12 To Bind to the Human IFN Receptor. We have shown previously (*27*) that the epitope ^{62}FSSLKLNVY^{70} recognized by the neutralizing anti-IFNAR1 mAb 64G12 is located in

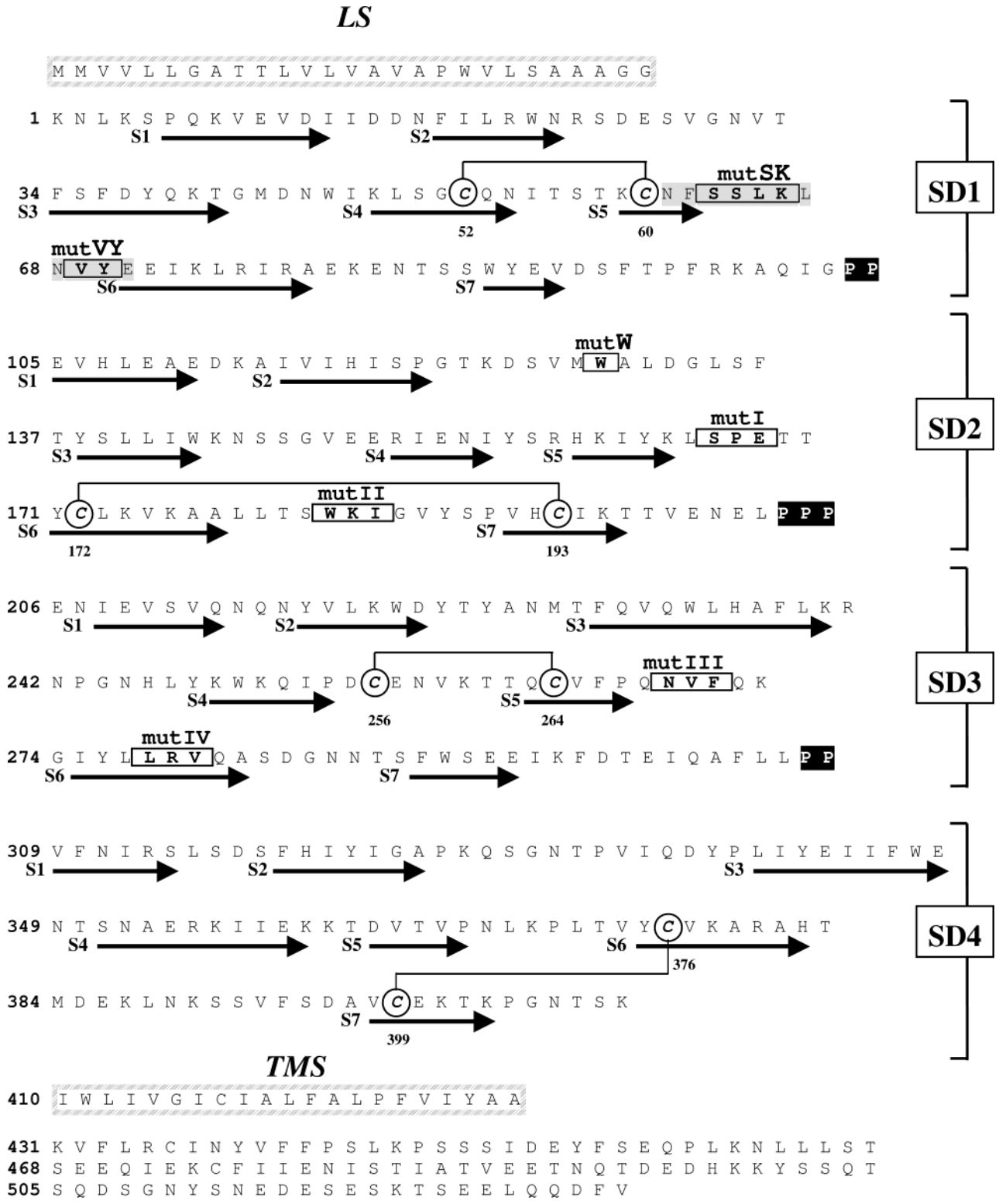

FIGURE 1: Location of mutated residues in the primary amino acid sequence of IFNAR1. Amino acid numbers are those of the mature polypeptide. SD1, SD2, SD3, and SD4 denote the four extracellular subdomains of IFNAR1 delimited by proline motifs (shaded black). Arrows denote putative β-strands predicted by the 3-D model presented herein and annotated S1, S2, S3, S4, S5, S6, and S7 for each IFNAR1 subdomain. Predicted disulfide bridges are annotated with circled cysteine (*C*) linked by bars. The epitope recognized by the 64G12 mAb is shaded gray. Each modified residue is indicated by emboldened upper case characters, and the designation of the mutated polypeptide is indicated above the sequence. Leader sequence is designated LS; transmembrane sequence is designated TMS.

the SD1 subdomain of IFNAR1. Thus, the 64G12 mAb failed to bind to cells expressing the IFNAR1 mutants ^{63}SSLK^{66} and ^{69}VY, even though they bound a second anti-IFNAR1 mAb, 34F10 (which recognizes a distant epitope on IFNAR1) in a manner similar to cells expressing the wild-type receptor (Figure 2). These findings confirm that the ^{62}FSSLKLNVY^{70} peptide is indeed the docking site for the 64G12 antibody including Fab′ fragments (data not shown) by virtue of which the antibody inhibits the biological activities of all type I human IFNs (*31*).

Cell Surface Expression of Human IFNAR1 and IFNAR2 in Mouse Transfectants. To ensure that observed effects on

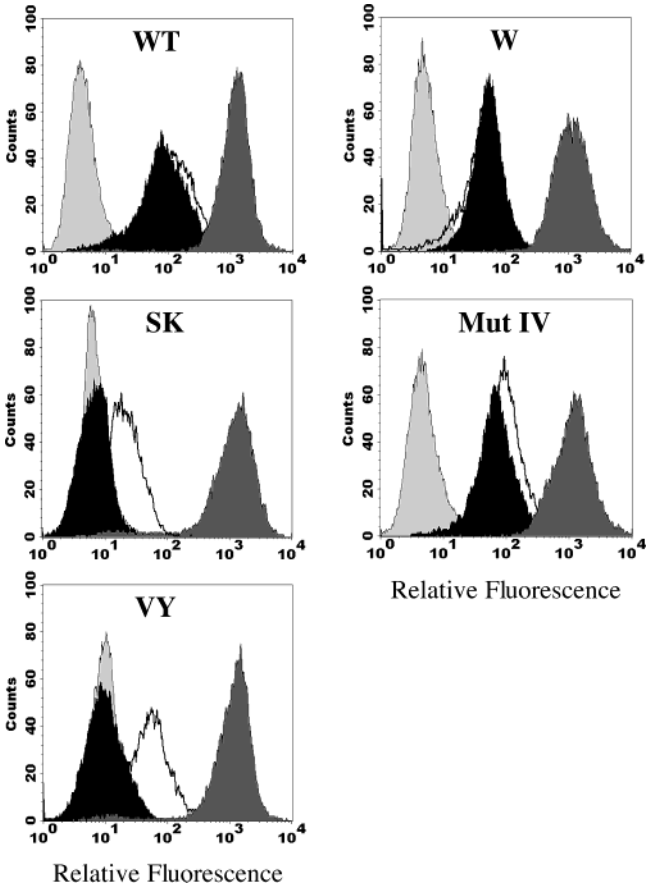

FIGURE 2: Expression of human IFNAR1 and IFNAR2 on the surface of mouse L929 cells transfected with wild-type or mutated IFNAR1. Two different anti-human IFNAR1 monoclonal antibodies, 64G12 and 34F10, and an anti-IFNAR2 mAb were used to monitor the expression of human IFNAR1 and IFNAR2, respectively, on the surface of transfected mouse L929 cells using flow cytometry. Light gray areas indicate background staining (secondary antibody alone), black areas indicate 64G12 binding, open areas 34F10 binding, and dark gray areas anti-IFNAR2 binding detected using a phycoerythrin-labeled secondary goat anti-mouse IgG antibody. Cell number is indicated on the ordinate and fluorescence intensity on the abcissa.

receptor binding do indeed reflect the effect of specific mutations in IFNAR1 on receptor binding, studies were carried out on transfectants expressing levels of IFNAR2 in excess of that of IFNAR1. Due to the high affinity of the human IFN receptor, binding studies were carried out using low concentrations of ligand. Thus, to facilitate comparison of binding curves under conditions where the IFNAR2 subunit was undersaturated, ligand binding data was expressed as the "occupied site ratio", which represents the amount of bound ligand, normalized with respect to the number of binding sites at saturation of the double transfectant expressing both IFNAR1 and IFNAR2, after subtraction of ligand binding to IFNAR2 alone (LR2 transfectant) at each IFN concentration, as described in the Experimental Procedures. Apparent binding constants (K_d) and the number of binding sites per cell were estimated by extrapolation of the linear portion of the Scatchard's plot for WT cells (Figure 3) and mutants SK and mutIV (Figures 4A and 5B). Because the binding curves for LR2 and mutants VY and W did not reach saturation at the concentrations of ligand employed, the number of binding sites per cell was estimated from the relative fluorescence intensity determined by flow cytometry

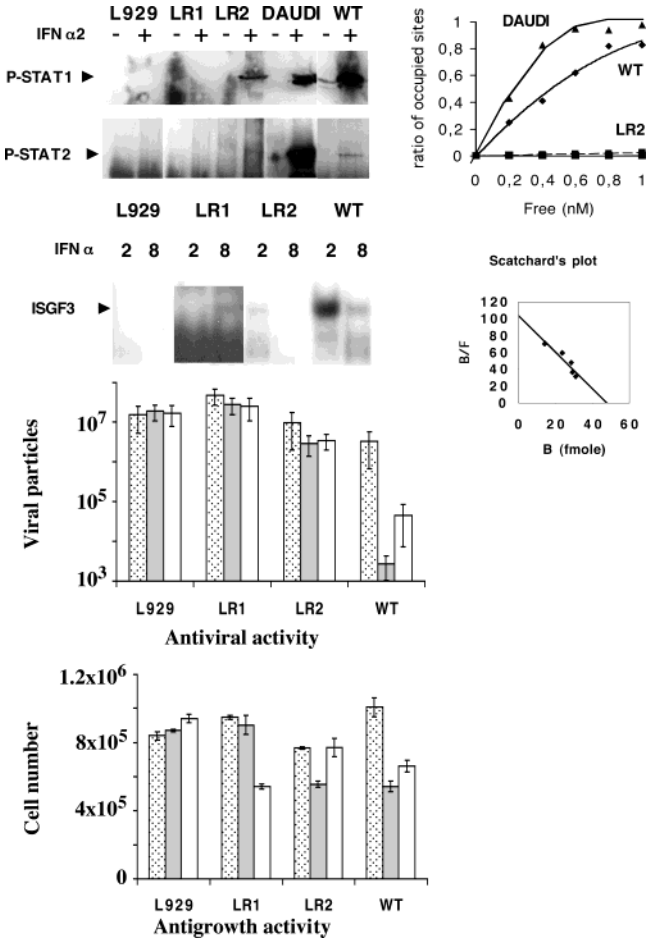

FIGURE 3: Binding of ^{125}I-HuIFN-α2 to the human interferon receptor expressed on mouse cells transfected with wild-type human IFNAR2 and IFNAR1 and various human IFNAR1 mutants. DAUDI denotes human cells, a positive control. L929, LR2, and WT denote recipient mouse L929 cells, human IFNAR2-transfected cells, and cells transfected with both wild-type human IFNAR1 and IFNAR2, respectively. L929 and IFNAR1-transfected mouse cells (LR1) gave binding plots superimposed with the abcissa (data not shown). To normalize the results obtained, receptor sites engaged in ^{125}I-IFN binding indicated on the ordinate were plotted versus the total number of IFNAR1 molecules estimated either by Scatchard's analysis or FACS, as indicated on the abcissa. In all cases, human IFNAR2 expression was in a 5−10-fold excess. Each curve represents the mean of five independent experiments. For induction of STAT1 and STAT2 tyrosine phosphorylation, murine L929 cells (10^6 per lane) transfected with human IFNAR1 and human IFNAR2 were treated (+) or not (−) with human IFN-α2 (1000 IU/mL) for 15 min at 37 °C. The cells were then lysed under reducing conditions as described in Experimental Procedures, and protein extracts were separated by SDS−8% PAGE, transferred to PVDF membranes, and probed with anti-phospho-STAT1 antibodies or immunoprecipitated with antibodies to STAT2, trapped with protein-G-Sepharose, and analyzed as above (2×10^7 cells per lane). PVDF membranes were probed with the anti-phospho-STAT2 antibody. ISGF3 complex formation following IFN activation was detected by EMSA assay using an ISRE probe as described in Experimental Procedures. Nuclear extracts were prepared from cells treated with 2000 IU/mL of human IFN-α2 or human IFN-α8. Untransfected murine L929, LR1, and LR2 cells expressing human IFNAR1 or human IFNAR2, respectively, were included as controls. For antiviral and antiproliferative activity, the bars indicate the antiviral and antiproliferative activities of IFN-a2 and IFN-a8 determined for cells transfected with human IFNAR1 (LR1) or human IFNAR2 (LR2) alone or L929 murine cells transfected with both IFNAR1 and IFNAR2 (WT). Control untreated cells are represented by dotted bars, IFN-α2-treated cells by gray bars, and IFN-α8-treated cells by empty bars.

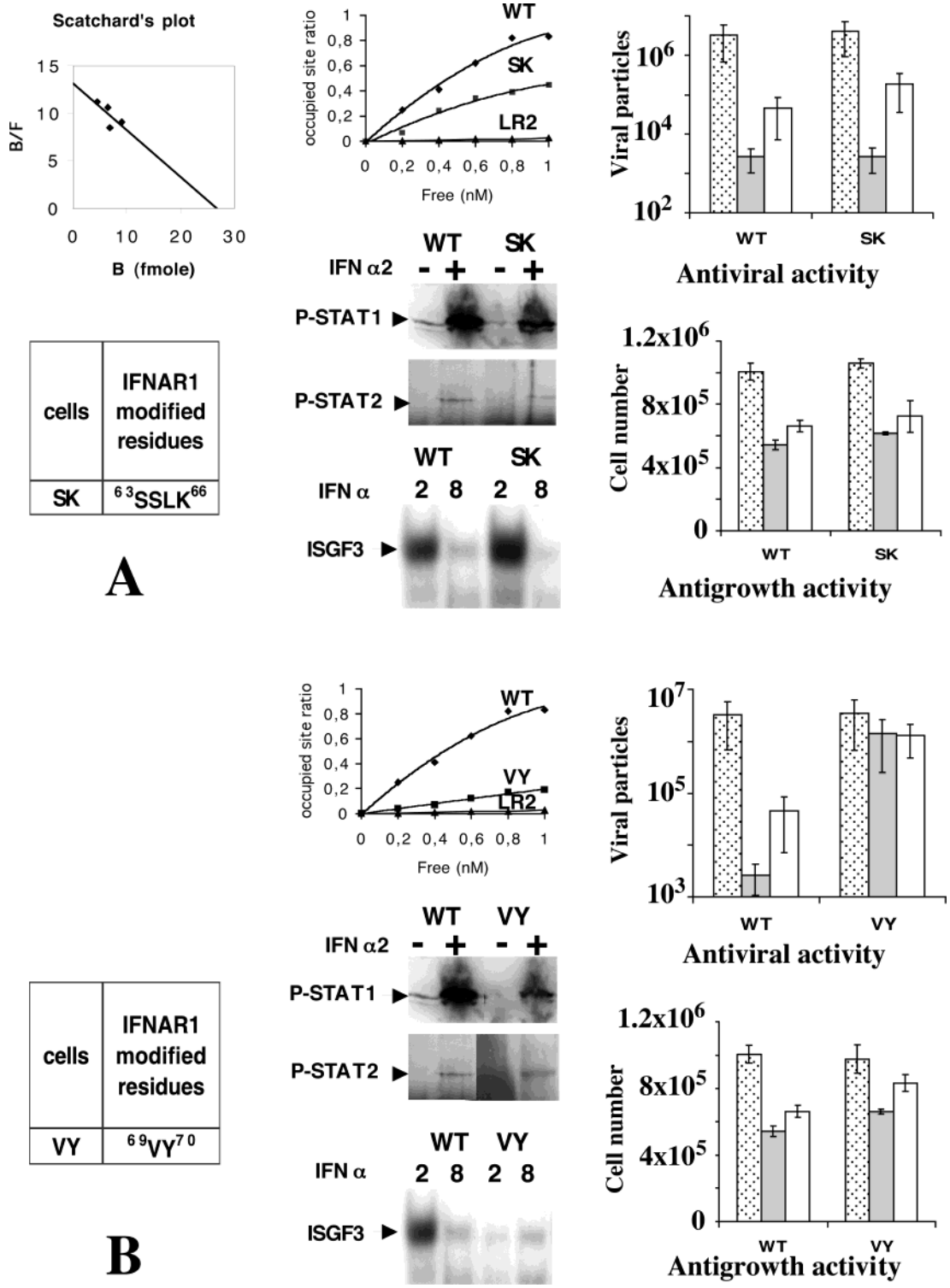

FIGURE 4: Binding and biological activities of IFNAR1 mutants SK (A, ^{63}SSLK^{66}) and VY (B, ^{69}VY). To normalize the results obtained, receptor sites engaged in ^{125}I-IFN binding indicated on the ordinate were plotted versus the total number of IFNAR1 molecules estimated either by Scatchard's analysis or FACS, as indicated on the abcissa. In all cases, human IFNAR2 expression was in a 5−10-fold excess. Each curve represents the mean of five independent experiments. For induction of STAT1 and STAT2 tyrosine phosphorylation, murine L929 cells (10^6 per lane) transfected with human IFNAR1 and human IFNAR2 were treated (+) or not (−) with human IFN-α2 (1000 IU/mL) for 15 min at 37 °C. The cells were then lysed under reducing conditions as described in Experimental Procedures, and protein extracts were separated by SDS−8% PAGE, transferred to PVDF membranes, and probed with anti-phospho-STAT1 antibodies or immunoprecipitated with antibodies to STAT2, trapped with protein-G-Sepharose, and analyzed as above (2×10^7 cells per lane). PVDF membranes were probed with the anti-phospho-STAT2 antibody. ISGF3 complex formation following IFN activation was detected by EMSA assay using an ISRE probe as described in Experimental Procedures. Nuclear extracts were prepared from cells treated with 2000 IU/mL of human IFN-α2 or human IFN-α8. For antiviral and antiproliferative activity, the bars indicate the antiviral and antiproliferative activities of IFN-a2 and IFN-a8 determined for L929 murine cells transfected with both IFNAR1 and IFNAR2. Control untreated cells are represented by dotted bars, IFN-α2-treated cells by gray bars, and IFN-α8-treated cells by empty bars.

Table 1: Binding Constants and Number of Receptor Sites[a]

cells	K_d (nM)	sites/cell	relative fluorescence	sites/cell fluor
L929		0	3.37	0
WT	0.45	31 000	45.32	
SK	1.40	17 000	25.03	
VY			88.17	65 000
W			42.55	29 000
mutIV	0.30	20 000	28.39	

[a] Apparent binding constants (K_d) and the number of receptor sites per cell (sites/cell) were determined for WT, SK, and mutIV transfectants from the slope and the abscissa intercept of the Scatchard's plot, respectively. Since the ligand binding curves for the VY and W transfectants did not reach saturation within the range of IFN doses tested, the number of receptor sites per cell (sites/cell fluor) was estimated from the mean relative fluorescence obtained using an anti-IFNAR1 mAb (64G12) taking the number of receptor sites per cell for WT, SK, and mutIV as reference values.

using anti-IFNAR2 and anti-IFNAR1 monoclonal antibodies by reference to the mean values obtained for WT cells and mutants SK and mutIV by Scatchard's analysis (Table 1).

Effect of Mutant SK on IFN Binding, Signal Transduction, and Induction of Biological Activity. Stable clones of mouse L929 cells transfected with the ^{63}SSLK^{66} mutant bound approximately 50% of either human recombinant IFN-α2, or IFN-α cons (data not shown) relative to the maximum binding observed for clones of mouse L929 cells stably transfected with the wild-type human IFNAR1 and IFNAR2 subunits (Figure 4A). Signal transduction following the binding of human IFN-α2, as determined by formation of phospho-STAT1, phospho-STAT2, or ISGF3 complexes, was unaffected in L929 cells transfected with the ^{63}SSLK^{66} mutant relative to cells transfected with the wild-type human receptor. Similarly, the antiviral and antiproliferative activities of IFN-α2 were unaffected in L929 cells transfected with the ^{63}SSLK^{66} mutant relative to cells transfected with the wild-type receptor (Figure 4A). A slight inhibition of ISGF3 complex formation and a reduction, albeit nonsignificant, in antiviral activity was observed when ^{63}SSLK^{66} mutant transfected cells were treated with IFN-α8 relative to cells transfected with the wild-type receptor (Figure 4A). Antiproliferative activity in cells transfected with the ^{63}SSLK^{66} mutant was similar to that observed in cells transfected with the wild-type receptor (Figure 4A).

Effect of Mutant VY on IFN Binding, Signal Transduction and Induction of Biological Activity. The second mutation, ^{69}VY, targeting the Y70 residue of the epitope recognized by the 64G12 neutralizing mAb, had a more marked effect on IFN binding, subsequent signal transmission, in particular with IFN-α2, and IFN-induced biological activity (Figure 4B). Thus, stable clones of mouse L929 cells transfected with the ^{69}VY mutant bound less than 20% of either human recombinant IFN-α2 or IFN-α cons (data not shown) relative to L929 cells transfected with WT human IFNAR1 (Figure 4B). These results demonstrate the importance of residue Y70 of the SD1 subdomain in ligand binding. Furthermore, STAT1 tyrosine phosphorylation was reduced to the baseline level (Figure 4B) observed with the LR2 mutant lacking the human IFNAR1 subunit following treatment with IFN-α2 (Figure 3). Similarly, ISGF3 complex formation was also reduced to the baseline level (Figure 4B) observed in extracts of the LR2 mutant, lacking the human IFNAR1 subunit, following treatment with IFN-α2 (Figure 3) but not with IFN-α8 (Figure 4B). No antiviral activity was detected following treatment of stable clones of mouse L929 expressing the ^{69}VY mutant with either human IFN-α2 or IFN-α8 (Figure 4B). Furthermore, no antiproliferative activity was detected following treatment of stable clones of mouse L929 expressing the ^{69}VY mutant with human IFN-α8, while a slight, albeit nonsignificant, activity was detected following treatment with human IFN-α2 (Figure 4B). These data suggest that the ^{69}VY residues in the SD1 subdomain of IFNAR1 are critical for IFN binding and induction of biological activity, in agreement with a previous report (*27*) showing that substitution of the Y70 residue abolishes the ability of the neutralizing monoclonal 64G12 to bind to IFNAR1.

Effect of the W129 Mutation on IFN Binding, Signal Transduction, and Induction of Biological Activity. The three-dimensional model for bovine IFNAR1, described by Cutrone and Langer (*18*), places the 64G12 epitope within 9−17 Å of residue W132 in SD2. According to the 3D homology model described herein, the corresponding tryptophan in the human IFNAR1 chain is situated at approximately 15 Å from Y70 in the epitope recognized by the 64G12 mAb. Residue W129 in the SD2 subdomain of human IFNAR1 was substituted with alanine, and stable transfectants of mouse L929 cells expressing the W129 mutant were isolated and tested for their ability to bind human IFN-α2. Although these transfectants exhibited an approximately 50% decrease in the binding of human IFN-α2 (Figure 5A) and a weak phospho-STAT1 signal relative to cells transfected with the wild-type receptor (Figure 5A), ISGF3 complex formation was comparable to that of cells transfected with the wild-type receptor following treatment with either IFN-α2 or IFN-α8 (Figure 5A), indicating that this single mutation does not significantly affect IFN-α signaling via the STAT1/STAT2 pathway. Surprisingly, even though ISGF3 complex formation appeared to be minimally affected, antiviral activity was completely inhibited (Figure 5A) and was comparable to the level observed with LR2 cells transfected with IFNAR2 alone (Figure 3). The antiproliferative activity of both IFN-α2 and IFN-α8 was unaffected, however, in cells transfected with mutant W relative to cells transfected with the WT receptor (Figure 5A). These results indicate that the conformational binding site formed between the epitope recognized by the 64G12 mAb in the SD1 subdomain and residue W129 in the SD2 subdomain is critical for the establishment of IFN-induced antiviral activity but not for the establishment of antiproliferative activity.

Effect of Mutant ^{278}LRV in Subdomain SD3 on IFN-α Binding, Signal Transduction, and Induction of Biological Activity. Substitution of the three amino acid cluster ^{278}LRV with alanine (mutant mutIV) in the S6 β-strand of the SD3 subdomain generates a mutant that exhibits full IFN-α binding in transfected L929 cells relative to cells expressing wild-type IFNAR1 (Figure 5B). In contrast, cells transfected with mutant mutIV exhibit a weak phospho-STAT1 signal and reduced ISGF3 complex formation in response to treatment with human IFN-α2 and no response at all to IFN-α8 even at doses up to 8000 IU/mL. In keeping with the observed inhibition of signal transduction, antiviral activity was also markedly inhibited in response to both human IFN-α2 and IFN-α8 (Figure 5B). A similar inhibition of IFN-

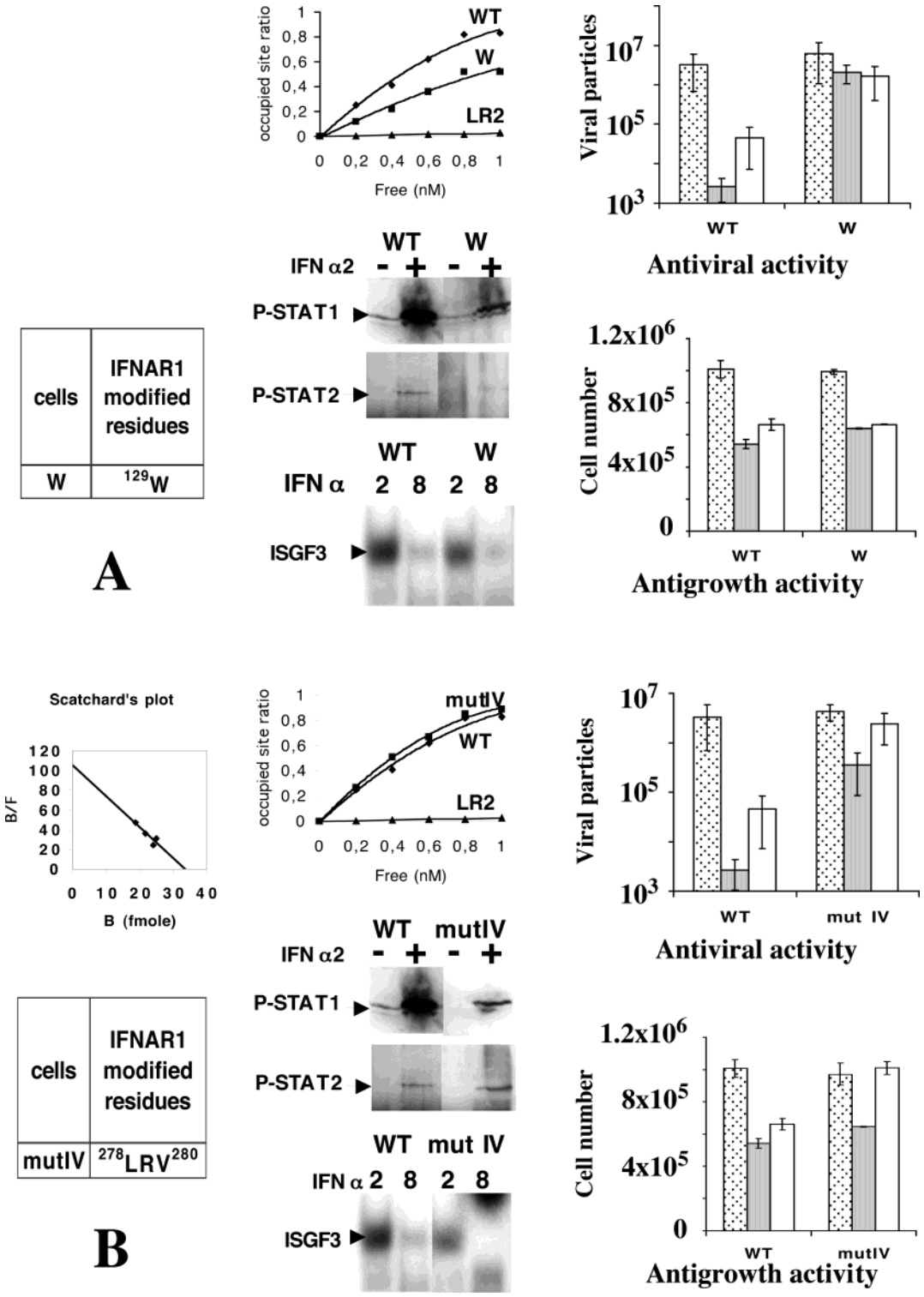

FIGURE 5: Binding and biological activities of IFNAR1 mutants W (A, ^{129}W) and mutIV (B, ^{278}LRV). To normalize the results obtained, receptor sites engaged in ^{125}I-IFN binding indicated on the ordinate were plotted versus the total number of IFNAR1 molecules estimated either by Scatchard's analysis or FACS, as indicated on the abcissa. In all cases, human IFNAR2 expression was in a 5−10-fold excess. Each curve represents the mean of five independent experiments. For induction of STAT1 and STAT2 tyrosine phosphorylation, murine L929 cells (10^6 per lane) transfected with human IFNAR1 and human IFNAR2 were treated (+) or not (−) with human IFN-α2 (1000 IU/mL) for 15 min at 37 °C. The cells were then lysed under reducing conditions as described in Experimental Procedures, and protein extracts were separated by SDS−8% PAGE, transferred to PVDF membranes, and probed with anti-phospho-STAT1 antibodies or immunoprecipitated with antibodies to STAT2, trapped with protein-G-Sepharose, and analyzed as above (2×10^7 cells per lane). PVDF membranes were probed with the anti-phospho-STAT2 antibody. ISGF3 complex formation following IFN activation was detected by EMSA assay using an ISRE probe as described in Experimental Procedures. Nuclear extracts were prepared from cells treated with 2000 IU/mL of human IFN-α2 or human IFN-α8. For antiviral and antiproliferative activity, the bars indicate the antiviral and antiproliferative activities of IFN-a2 and IFN-a8 determined for L929 murine cells transfected with both IFNAR1 and IFNAR2. Control untreated cells are represented by dotted bars, IFN-α2-treated cells by gray bars, and IFN-α8-treated cells by empty bars.

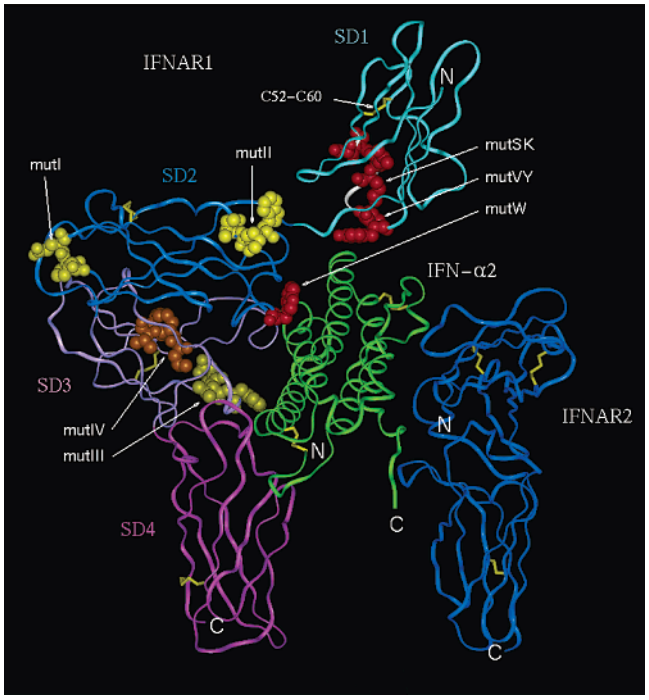

FIGURE 6: Ribbon representation of the 3-D homology model for the ternary IFN-α2/IFNAR1/IFNAR2 complex. IFN-α2 (green), IFNAR2 (deep blue), and SD1 (sky blue), SD2 (blue), SD3 (pink), and SD4 (magenta) subdomains of IFNAR1 are represented. The 64G12 epitope ^{62}FSSLKLNVY^{70} peptide is represented as a white ribbon. Predicted disulfide bridges are depicted in yellow, and the disulfide bridge formed by residues C52−C60 is indicated. Side chains of mutated residues are displayed in CPK (Corey, Pauling, Kultan color scheme): in red, ^{63}SSLK, ^{69}VY, and ^{129}W mutations; in yellow, ^{166}SPE (mutI), ^{183}WKI (mutII), and ^{269}NVF (mutIII); in orange, ^{278}LRV (mutIV). N and C denote the N-terminal and C-terminal ends, respectively, of IFNAR1, IFNAR2, and IFN-α2.

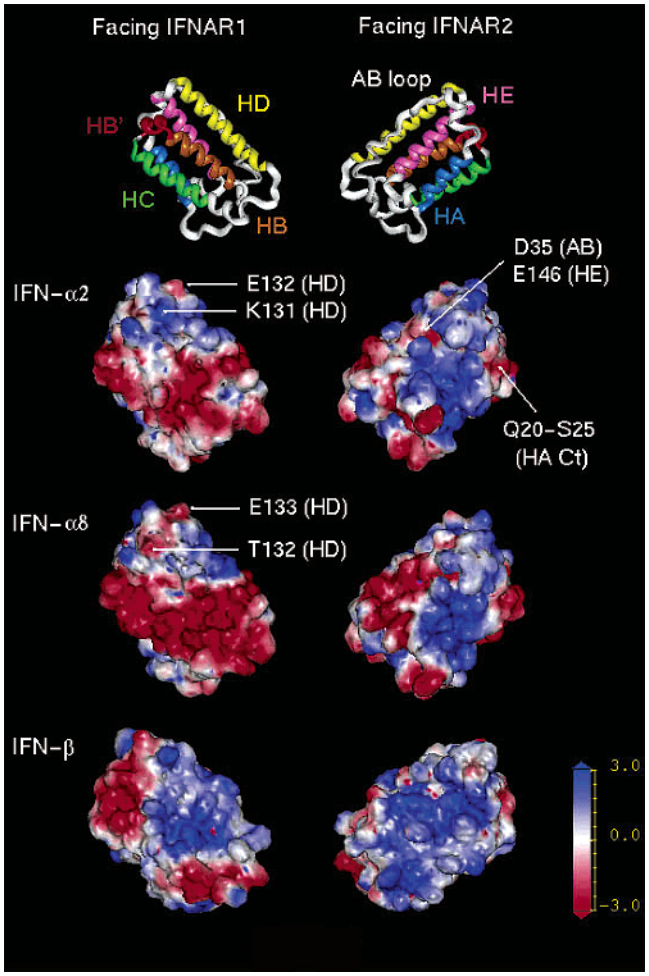

FIGURE 7: Electrostatic potentials of the surface of IFN-α2, IFN-α8, and IFN-β, which interact with IFNAR1 and IFNAR2. Each column shows the surface of the different IFN subtypes interacting with either IFNAR1 (left) or IFNAR2 (right). At the top of the figure is a graphic representation of the structure of human IFN-α2 indicating the position of α-helices and β-sheets. Secondary structures are color-coded as follows: helix A (HA), blue; helix B (HB), orange; helix C (HC), green; helix D (HD), yellow; helix E (HE), magenta. Helix B′ (HB′) in the BC loop is colored red. In the lower part of the figure, electrostatic potentials of IFN-α2, IFN-α8, and IFN-β are depicted in the same orientation as the structure of IFN-α2 depicted at the top. The structure of IFN-β was derived from the PDB databank (code 1au1; *61*).

induced antiproliferative activity was also observed in mouse L929 cells transfected with mutant mutIV following treatment with IFN-α8 where antiproliferative activity was completely inhibited relative to cells transfected with the wild-type receptor (Figure 5B). The observation that this mutation does not affect IFN-α2 (Figure 5B) or IFN-cons (data not shown) binding suggests that binding of IFN to its receptor can be uncoupled from the establishment of certain biological activities for a particular subspecies of IFN-α. Similar results were obtained for three different stable clones of mutIV suggesting that this observation is not specific to a particular clone of cells.

The remaining mutants designated mutI (^{166}SPE), mutII (^{183}WK) in SD2, and mutIII (^{269}NVF) in the SD3 subdomain of IFNAR1 generated minor differences in IFN-α2 binding, signal transduction, and biological activity in the stable transfectants tested.

Modeling of the IFN-α2/IFNAR1/IFNAR2 Complex. The homology model for the extracellular domain of IFNAR1 (Figure 6) was generated as described in the Experimental Procedures. The extracellular domains of human IFNAR1 and IFNAR2 adopt structures containing four and two FNIII subdomains, respectively, each composed of seven β-strands distributed in two sheets. IFNAR1 contains four potential disulfide bonds (C52−C60, C172−C193, C256−C264, and C376−C399).

The model of the human IFN-α2/IFNAR2 complex described herein was constructed from the results of double-mutant experiments (*21*) describing pairs of interacting residues between IFN-α2 and IFNAR2 (see Experimental Procedures). Electrostatic potential calculations demonstrated charge complementarities between IFN-α2 and human IFNAR2. Indeed, the interacting surface of IFN-α2 encompasses the E helix and the AB loop and consists of a positive potential surface with two small negative patches corresponding to the ^{20}QMRKIS^{25} fragment and D35/E146 residues (Figure 7). In our model, they are matched with two positive clusters located in human IFNAR2 (K75 and K80 residues) surrounded by a large negative potential surface.

The surface of the IFN-α2 protein opposite the contact surface with IFNAR2 is thought to bind the IFNAR1 chain (*29*); IFN-α electrostatic potentials display a large negative potential surface roughly distributed along helix C and in the N-terminal of helix B, while a positive patch is located at the C-terminal of helix B (Figure 7). The SD3 and SD4

Table 2: Genotype and Phenotype of the IFNAR1 Mutants Studied[a]

mutant	IFNAR1 modified residue	relative binding (IFNα2)	ISGF3 formation		antiviral activity		antiproliferative activity (% growth)	
			IFN-α2	IFN-α8	IFN-α2	IFN-α8	IFN-α2	IFN-α8
L929		0	−	−	−	−	100	100
LR2		1	+	−	−	−	75	100
LR1	none	0	−	+	−	−	95	58
WT	none	100	+++	+	+++	++	55	65
SK	^{63}SSLK^{66}	50	+++	+	+++	+	60	70
VY	^{69}VY^{70}	20	+	+	−	−	72	85
W	^{129}W	50	+++	+	−	−	65	67
mutIV	^{278}LRV^{280}	100	+	−	+	−	65	100

[a] Results for ISGF3 complex formation and antiviral activity during IFN activation were expressed as full (+++), partial (++), weak (+), or not detected (−).

subdomains of IFNAR1 were docked on the IFN-α2 structure according to electrostatic potential complementarities and mutagenesis data performed on tyrosine residues located in helix C (*25*). In our model, the human IFNAR1 SD4 subdomain interacts with the central part of the C helix of IFN-α2 when the major interaction site of the SD3 subdomain is located in the BC loop and in particular on the small B′ helix (^{70}KDSSA^{74}).

In class II cytokine receptor complexes of known structure, only two subdomains of the receptor are required to interact with the ligand, suggesting that the SD1 and SD2 subdomains of IFNAR1 may not bind IFN-α. This model would predict an "open form" of the IFN-α/IFNAR1/IFNAR2 complex. The observation that the epitope recognized by the 64G12 antibody (^{62}FSSLKLNVY^{70}) in SD1 can interact with IFN-α2 suggests a "closed form" of the IFN-α/IFNAR1/IFNAR2 complex in which all four IFNAR1 subdomains interact with IFN-α. Consequently, the SD1 and SD2 subdomains of IFNAR1 would be docked on IFN-α2. Thus, with the use of electrostatic potentials and the results of mutagenesis studies involving several aromatic residues (*18*), SD2 was positioned so as to interact with residues from both C-terminal regions of the B and D helices of IFN-α. Finally, we chose to dock the loop in the SD1 subdomain of IFNAR1 enclosing the 64G12 epitope with IFN residues located at the C-terminal of helix D (Figure 6). This is in agreement with Schmeisser et al., (*41*) who showed that amino acid substitutions in loop BC, helix C, and helix D alter the interaction between IFN-α and its receptor and influence the threshold of activation of the biological response.

DISCUSSION

Elucidation of the role played by IFNAR1 in the binding of type I IFNs to their high-affinity cell-surface receptor has been limited by the low affinity of IFN-α for recombinant IFNAR1 (*6* and Eid, P., unpublished results). In this study, we have attempted to obviate these difficulties by the use of mutation analysis to identify critical residues involved in IFN−receptor interactions.

Residues predicted to be critical for ligand binding were mutated to alanine, and mouse L929 cells transfected with mutated human IFNAR1 and wild-type human IFNAR2 were tested for IFN binding, signal transduction, and biological activity (Table 2). Although mouse L929 cells do not bind detectable amounts of most human type-I IFNs and do not respond to human IFN-α2 or IFN-α8, they contain a functional signaling apparatus and respond to human IFN following transfection with the human type I IFN receptor. Thus, this system has been used extensively to study human IFN−receptor interactions and signal transduction. The IFNAR1 chain of the human type I IFN receptor does not act as an independent and passive docking site for IFN since it has been shown that association with the Tyk2 tyrosine kinase is a prerequisite for functional high-affinity ligand binding and for stabilizing IFNAR1 expression at the cell surface (*42*, *43*). Indeed, there even appears to be some interaction between IFNAR1 and components of the IFN-γ receptor signaling pathway, as the IFN-γ-induced antiviral response is impaired in IFNAR1-null cells (*44*). The conformation of IFNAR1 also appears to be critical for functional receptor expression. Cysteine 60 in the SD1 subdomain of IFNAR1 is highly conserved, and attempts to mutate this residue to alanine and generate stable clones have failed, most likely because this substitution disrupts an essential disulfide bond (predicted between C52 and C60) leading to a conformational change that interferes with the correct expression of the receptor polypeptides on the cell surface.

Reduction in signaling events observed with the transfectants is likely underestimated if we take into account the basal signaling level, in particular phospho-STAT1 induction, observed in mouse cells transfected with human IFNAR2 alone. It has been shown previously that differences in induction of an antiviral state by IFN-α and IFN-β may not correlate with differences in activation of the JAK−STAT pathway (*45*, *46*).

Residues of mutants ^{63}SSLK^{66} and ^{69}VY in the SD1 subdomain and mutant W129 in the SD2 subdomain of human IFNAR1 were mutated to determine the role of the epitope (^{62}FSSLKLNVY^{70}) recognized by the neutralizing monoclonal antibody 64G12 in ligand binding (*27*). Substitution of residues ^{69}VY with alanine led to a more than 80% decrease in IFN-α2 binding and abolished IFN-induced antiviral activity, suggesting that these residues situated in the S5−S6 loop of the SD1 subdomain of human IFNAR1 are indeed involved in ligand binding, most probably of all type I IFNs, since the 64G12 antibody, which recognizes this epitope, inhibits the binding of all type I IFNs (*31*).

In contrast, the homologous sequence, ^{62}FSSVELENVF^{71}, in bovine IFNAR1 was shown by mutation analysis to play a relatively modest role in the binding of heterologous human IFN-α2 (*18*). Thus, although the SD1 subdomain of IFNAR1 may well play a minor role in the cross-species binding of IFNs as suggested previously (*30*), the results presented herein suggest that the SD1 subdomain of human IFNAR1 is directly involved in ligand binding. These results are in

keeping with previous results showing that the neutralizing anti-IFNAR1 monoclonal antibody 4A7 binds to the SD1 subdomain of IFNAR1 and that the more strongly neutralizing anti-IFNAR1 antibody 2E1 binds to both the SD1 and SD2 subdomains (*26*) suggesting that both subdomains are involved in IFN binding.

Mogensen et al. (*47*) proposed a putative two-site model for type-I IFN binding in which two IFN molecules would bind to a flexible IFNAR1 molecule curved in such a manner that its N-terminus was close to the plasma membrane and facing two IFNAR2 molecules. It is difficult to explain such a two-site model in light of our results, which show that substitution of the two amino acids ^{69}VY in the SD1 subdomain or a single amino acid, W129, in the SD2 subdomain both lead to inhibition of IFN-α-induced biological activity. In addition, the neutralizing monoclonal antibody 64G12, which recognizes a single linear epitope within the SD1 subdomain of IFNAR1, completely inhibits IFN binding to the cell surface receptor (*27*, *31*). The results presented herein show that ^{62}FSSLKLNVY^{70} is the unique epitope recognized by this antibody and that substitution of alanine in residues ^{63}SSLK^{66} or ^{69}VY abrogates the blocking activity of the antibody.

It is generally accepted that the biological effects elicited by a given IFN are directly proportional to the affinity of the IFN for its cell surface receptor. The results presented show, however, that mutation ^{278}LRV in the SD3 subdomain inhibits signal transduction and the establishment of both antiviral and antiproliferative activity in the absence of a significant effect on the binding of IFN-α to the receptor complex. These results show that IFN binding can be uncoupled from the establishment of biological activity, suggesting that the positively charged arginine at position 279 plays an important role in the induction of IFN-induced biological activity.

The 3-D model of the human IFN receptor complex presented herein was constructed to elucidate ligand−receptor interactions and to identify residues of the IFNAR1 chain critical for IFN binding and the establishment of biological activity. When hydrophobic α-helices and β-sheets form the core of a protein, it is accepted that turns and loops are generally exposed at the surface, rendering them more likely to be involved in the biological function of the protein than unexposed regions. All the residues mutated in the SD2 and SD3 subdomains of IFNAR1 were within hydrophilic turns and loops at the surface of the protein, with the exception of mutation mutIV (^{278}LRV), which lies in the middle of a β-strand. The model that we have developed using different methods, reinforces that proposed by Piehler et al. (*24*).

Substitution of residue W129 with alanine was found to reduce IFN binding and phosphorylation of STAT1 and to markedly inhibit antiviral activity even though ISGF3 complex formation was only slightly reduced. These results suggest that residue W129 in the SD2 subdomain is critical for the establishment of IFN-induced antiviral activity and may be involved in receptor signaling through a pathway(s) other than the JAK−STAT pathway. Previous studies have shown that components of multiple signaling pathways in addition to the JAK−STAT pathway are activated following binding of IFN-α to its cell-surface receptor. These include the insulin-receptor substrate (*48*), phosphatidyl-inositol 3′-kinase (*49*), Crk-proteins (*50*), and mitogen-activated protein (Map) kinases (*51*, *52*). Furthermore, the antiviral activity of type I interferons is reduced in cells with targeted disruption of the MapKapK-2 gene (*53*) suggesting that the p38 Map kinase pathway participates in downstream signaling following receptor binding.

Thus, the ability of the 64G12 mAb to inhibit the biological activity of the type I IFNs may be due to its ability to block the conformational binding site formed between the epitope recognized by the 64G12 mAb in the SD1 subdomain and residue W129 in the SD2 subdomain. Interestingly, it has been reported that the affinity of another neutralizing anti-IFNAR1 mAb (2E1) was markedly reduced when the peptide ^{71}EEIKLR^{76} in the SD1 subdomain was mutated (*26*). The ^{71}EEIKLR^{76} peptide is situated immediately after residue Y70 of the 64G12 epitope (^{62}FSSLKLNVY^{70}). The 64G12 antibody is also able to neutralize IFN-β, in addition to the different IFN-α subtypes, in contrast to the 2E1 mAb, suggesting that W129 and Y70 may be involved in the binding of both IFN-α and IFN-β to the receptor complex.

In addition, the 3-D model that we have constructed predicts that Y70 (mutVY), W129 (mutW), and K66 (mutSK), are involved in IFN binding. The distances calculated between the mutated residues of the 64G12 epitope on IFNAR1 and an interferon molecule are 5 Å between Y70 and helix D, 6 Å between W129 and helix D, and 6 Å between K66 and the interferon molecule.

Our results suggest that both the IFNAR1 and IFNAR2 receptor chains are most likely anchored in the plasma membrane in close proximity prior to ligand activation; otherwise, it is difficult to explain how IFNAR1-specific monoclonal antibodies such as 64G12 or EA12 (*54*), that do not affect binding of IFN-α to isolated IFNAR2, block type-I IFN binding to the whole receptor and inhibit the establishment of antiviral activity. Thus, these results suggest that prior to ligand binding IFNAR1 and IFNAR2 adopt an unproductive conformation, which upon initial IFN binding assumes a productive conformation, leading to a high-affinity interaction and the subsequent activation of receptor-associated cytoplasmic tyrosine kinases of the JAK family (JAK1, Tyk2). It is interesting to note that a recent study using FRET technology allowing real-time monitoring of high/low-affinity receptor interactions in the plasma membrane of living cells demonstrated that the two IFN-γ receptor chains are preassociated in the cell membrane prior to IFN-γ binding, raising the possibility that the subunits of other interferon receptors are preassociated prior to ligand binding (*55*).

The model presented herein sheds new light on the structure of the ternary IFN-α/IFN-receptor complex and identifies a number of specific IFN-α-binding domains on the surface of the receptor in keeping with previous data from other laboratories. In particular, this model provides insight into the interactions between the SD1 subdomain of IFNAR1 and IFN-α. The model also provides a basis for an understanding of how differences in the electrostatic potential distribution on the surface of IFN molecules may explain differences in receptor binding between different IFN-α subtypes. It has been reported, for example, that IFN "consensus" has a higher affinity for the IFN receptor than IFN-α2 or IFN-α8 (*56*), and several studies have shown that the antiviral activity of IFN-cons is higher than that of IFN-α2 or IFN-α8 (*57*, *58*). Moreover, Hu et al. (*59*, *60*) ranked

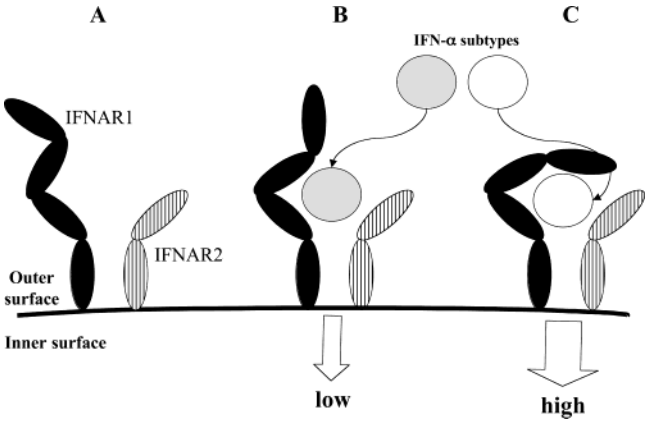

FIGURE 8: Proposed mechanism for IFN−receptor complex activation: (A) IFNAR1 and IFNAR2 chains are assumed to be preassociated on the cell surface; (B) an IFN-α subtype binds to the receptor complex, which adopts a progressively closed form leading to a low level of intracellular signaling; (C) binding of a different IFN-α subtype induces a more tightly closed form of the receptor complex leading to a higher level of intracellular signaling.

various IFN-α subtypes in terms of antiproliferative activity. The interaction of IFN-α8 and IFN-*β* with the human type I IFN receptors was evaluated from the distribution of their electrostatic potentials and an analysis of the binding surfaces on IFN-α2 for human IFNAR1 and IFNAR2. Although, these potentials are very similar for both IFN-α subtypes compared to IFN-*β*, which is more electropositive (Figure 7), slight differences between the two IFN-α subtypes were observed for the surface interaction with IFNAR1: Helix C is more electronegative for IFN-α8 than for IFN-α2. Although such indications suggest that all IFN-α subtypes may bind the receptor complex with the same orientation and at a similar site, in the 3-D model presented herein, the SD1 subdomain of IFNAR1 is in close proximity to the C end of helix D (particularly residue E132 in IFN-α2 or the corresponding residue E133 in IFN-α8). The electrostatic environment of this glutamate is different, however, in IFN-α2 where an electropositive cluster surrounds the electronegative cluster corresponding to the glutamate, whereas in IFN-α8 this cluster is more extended, due to the presence of the T132 residue in IFN-α8 instead of the K131 residue in IFN-α2 (Figure 7). Furthermore, the ^{63}SSLK^{66} mutant loses the positive charge due to the presence of the K66 residue. Both the increase in the electronegativity of IFN-α8 relative to IFN-α2 and the loss of the positive charge in the mutated receptor may well account for a change in receptor/ligand stability, depending upon the IFN-α subtype that binds to the mutated receptor.

Given the conserved protein structure of the IFN-α subtypes and the observation that all IFN-α subtypes compete for a common binding site, the model presented herein predicts that differences in the primary sequences of different IFN-α molecules modulate their binding affinity, the duration of the ligand/receptor association, or both. These parameters may also be responsible for the ability of the interferon receptor to adopt a stable closed conformation.

In conclusion, a dynamic mechanism for the IFN-α/receptor complex activation has been proposed that provides insight into the organization of the human type I IFN receptor and in particular the role played by the IFNAR1 chain in IFN binding (Figure 8). This mechanism predicts that IFNAR1 and IFNAR2 are most probably anchored in close proximity on the cell surface and that upon IFN binding the complex adopts a progressively more closed form resulting in the activation of intracellular kinases. Thus, differences in the binding affinities of individual IFN-α subtypes and the stability of the resulting IFN−receptor complex would explain the differences in intracellular signal intensities observed for individual IFN-α subtypes resulting from variations in sequential thresholds of activation.

REFERENCES

1. Chill, J. H., Quadt, S. R., Levy, R., Schreiber, G., and Anglister, J. (2003) The human type I interferon receptor: NMR structure reveals the molecular basis of ligand binding, *Structure 11*, 791−802.
2. Bazan, J. F. (1990) Structural design and molecular evolution of a cytokine receptor superfamily *Proc. Natl. Acad. Sci. U.S.A. 87*, 6934−6938.
3. Kotenko, S. V., Gallagher, G., Baurin, V. V., Lewis-Antes, A., Shen, M., Shah, N. K., Langer, J. A., Sheikh, F., Dickensheets, H., and Donnelly, R. P. (2003) IFN-lambdas mediate antiviral protection through a distinct class II cytokine receptor complex, *Nat. Immunol. 4*, 69−77.
4. Sheppard, P., Kindsvogel, W., Xu, W., Henderson, K., Schlutsmeyer, S., Whitmore, T. E., Kuestner, R., Garrigues, U., Birks, C., Roraback, J., Ostrander, C., Dong, D., Shin, J., Presnell, S., Fox, B., Haldeman, B., Cooper, E., Taft, D., Gilbert, T., Grant, F. J., Tackett, M., Krivan, W., McKnight, G., Clegg, C., Foster, D., and Klucher, K. M. (2003) IL-28, IL-29 and their class II cytokine receptor IL-28R, *Nat. Immunol. 4*, 63−68.
5. Cook, J. R., Cleary, C. M., Mariano, T. M., Izotova, L., and Pestka, S. (1996) Differential responsiveness of a splice variant of the human type I interferon receptor to interferons, *J. Biol. Chem. 271*, 13448−13453.
6. Cutrone, E. C., and Langer, J. A. (1997) Contributions of cloned type I interferon receptor subunits to differential ligand binding, *FEBS Lett. 404*, 197−202.
7. Lutfalla, G., Holland, S. J., Cinato, E., Monneron, D., Reboul, J., Rogers, N. C., Smith, J. M., Stark, G. R., Gardiner, K., Mogensen, K. E., Kerr, I. M., and Uzé, G. (1995) Mutant U5A cells are complemented by an interferon-alpha beta receptor subunit generated by alternative processing of a new member of a cytokine receptor gene cluster, *EMBO J. 14*, 5100−5108.
8. Domanski, P., Witte, M., Kellum, M., Rubinstein, M., Hackett, R., Pitha, P., and Colamonici, O. R. (1995) Cloning and expression of a long form of the beta subunit of the interferon alpha beta receptor that is required for signaling, *J. Biol. Chem. 270*, 21606−21611.
9. Piehler, J., and Schreiber, G. (1999) Mutational and structural analysis of the binding interface between type I interferons and their receptor ifnar2, *J. Mol. Biol. 294*, 223−237.
10. Arduini, R. M., Strauch, K. L., Runkel, L. A., Carlson, M. M., Hronowski, X., Foley, S. F., Young, C. N., Cheng, W., Hochman, P. S., and Baker, D. P. (1999) Characterization of a soluble ternary complex formed between human interferon-beta-1a and its receptor chains, *Protein Sci 8*, 1867−1877.
11. Domanski, P., and Colamonici, O. R. (1996) The type-I interferon receptor. The long and short of it, *Cytokine Growth Factor Rev. 7*, 143−151.
12. Langer, J., Garotta, G., and Pestka, S. (1996) Interferon receptors, *Biotherapy 8*, 163−174.
13. Uzé, G., Lutfalla, G., and Gresser, I. (1990) Genetic transfer of a functional human interferon alpha receptor into mouse cells: cloning and expression of its cDNA, *Cell 60*, 225−234.
14. Novick, D., Cohen, B., and Rubinstein, M. (1994) The human interferon alpha/beta receptor: characterization and molecular cloning, *Cell 77*, 391−400.
15. Ihle, J. N., and Kerr, I. M. (1995) Jaks and Stats in signaling by the cytokine receptor superfamily, *Trends Genet. 11*, 69−74.
16. Darnell, J. E. (1997) STATs and gene regulation, *Science 277*, 1630−1635.

17. Seto, M. H., Harkins, R. N., Adler, M., Whitlow, M., Church, W. B., and Croze, E. (1995) Homology model of human interferon-alpha 8 and its receptor complex, *Protein Sci. 4*, 655−670.
18. Cutrone, E. C., and Langer, J. A. (2001) Identification of critical residues in bovine IFNAR-1 responsible for interferon binding, *J. Biol. Chem. 276*, 17140−17148.
19. Lewerenz, M., Mogensen, K. E., and Uzé, G. (1998) Shared receptor components but distinct complexes for alpha and beta interferons, *J. Mol. Biol. 282*, 585−599.
20. Chill, J. H., Nivasch, R., Levy, R., Albeck, S., Schreiber, G., and Anglister, J. (2002) The human interferon receptor: NMR-based modeling, mapping of the IFN-alpha 2 binding site, and observed ligand-induced tightening, *Biochemistry 41*, 3575−3585.
21. Roisman, L. C., Piehler, J., Trosset, J. Y., Scheraga, H. A., and Schreiber, G. (2001) Structure of the interferon-receptor complex determined by distance constraints from double-mutant cycles and flexible docking, *Proc. Natl. Acad. Sci. U.S.A. 98*, 13231−13236.
22. Uzé, G., Di Marco, S., Mouchel-Vielh, E., Monneron, D., Bandu, M. T., Horisberger, M. A., Dorques, A., Lutfalla, G., and Mogensen, K. E. (1994) Domains of interaction between alpha interferon and its receptor components, *J. Mol. Biol. 243*, 245−257.
23. Runkel, L., Pfeffer, L., Lewerenz, M., Monneron, D., Yang, C. H., Murti, A., Pellegrini, S., Goelz, S., Uzé, G., and Mogensen, K. (1998) Differences in activity between alpha and beta type I interferons explored by mutational analysis, *J. Biol. Chem. 273*, 8003−8008.
24. Piehler, J., Roisman, L. C., and Schreiber, G. (2000) New structural and functional aspects of the type I interferon-receptor interaction revealed by comprehensive mutational analysis of the binding interface, *J. Biol. Chem. 275*, 40425−40433.
25. Hu, R., Bekisz, J., Schmeisser, H., McPhie, P., and Zoon, K. (2001) Human IFN-alpha protein engineering: the amino acid residues at positions 86 and 90 are important for antiproliferative activity, *J. Immunol. 167*, 1482−1489.
26. Lu, J., Chuntharapai, A., Beck, J., Bass, S., Ow, A., Devos, A. M., Gibbs, V., and Kim, K. J. (1998) Structure−function study of the extracellular domain of the human IFN-alpha receptor (hIFNAR1) using blocking monoclonal antibodies: The role of domains 1 and 2, *J. Immunol. 160*, 1782−1788.
27. Eid, P., Langer, J. A., Bailly, G., Lejealle, R., Guymarho, J., and Tovey, M. G. (2000) Localization of a receptor nonapeptide with a possible role in the binding of the type I interferons, *Eur. Cytokine Network 11*, 560−573.
28. Chuntharapai, A., Gibbs, V., Lu, J., Ow, A., Marsters, S., Ashkenazi, A., De Vos, A., and Jin Kim, K. (1999) Determination of residues involved in ligand binding and signal transmission in the human IFN-alpha receptor 2, *J. Immunol. 163*, 766−773.
29. Runkel, L., deDios, C., Karpusas, M., Betzenhauser, M., Muldowney, C., Zafari, M., Benjamin, C. D., Miller, S., Hochman, P. S., and Whitty, A. (2000) Systematic mutational mapping of sites on human interferon-beta-1a that are important for receptor binding and functional activity, *Biochemistry 39*, 2538−2551.
30. Kumaran, J., Colamonici, O. R., and Fish, E. N. (2000) Structure−function study of the extracellular domain of the human type I interferon receptor (IFNAR)-1 subunit, *J. Interferon Cytokine Res. 20*, 479−485.
31. Benoit, P., Maguire, D., Plavec, I., Kocher, H., Tovey, M., and Meyer, F. (1993) A monoclonal antibody to recombinant human IFN-alpha receptor inhibits biologic activity of several species of human IFN-alpha, IFN-beta, and IFN-omega. Detection of heterogeneity of the cellular type I IFN receptor, *J. Immunol. 150*, 707−716.
32. Mogensen, K. E., and Uzé, G. (1986) Radioiodination of human alpha interferons by the chloramine T method, *Methods Enzymol. 119*, 267−276.
33. Klotz, I. M., and Hunston, D. L. (1984) Mathematical models for ligand−receptor binding. Real sites, ghost sites, *J. Biol. Chem. 259*, 10060−10062.
34. Sali, A., and Blundell, T. L. (1993) Comparative protein modelling by satisfaction of spatial restraints, *J. Mol. Biol. 234*, 779−815.
35. Randal, M., and Kossiakoff, A. A. (2001) The structure and activity of a monomeric interferon-gamma: alpha-chain receptor signaling complex, *Structure 9*, 155−163.
36. Muller, Y. A., Ultsch, M. H., and de Vos, A. M. (1996) The crystal structure of the extracellular domain of human tissue factor refined to 1.7 Å resolution, *J. Mol. Biol. 256*, 144−159.
37. Callebaut, I., Labesse, G., Durand, P., Poupon, A., Canard, L., Chomilier, J., Henrissat, B., and Mornon, J. P. (1997) Deciphering protein sequence information through hydrophobic cluster analysis (HCA): current status and perspectives, *Cell. Mol. Life Sci. 53*, 621−645.
38. Luthy, R., Bowie, J. U., and Eisenberg, D. (1992) Assessment of protein models with three-dimensional profiles, *Nature 356*, 83−85.
39. Klaus, W., Gsell, B., Labhardt, A. M., Wipf, B., and Senn, H. (1997) The three-dimensional high-resolution structure of human interferon alpha-2a determined by heteronuclear NMR spectroscopy in solution, *J. Mol. Biol. 274*, 661−675.
40. Uzé, G., Lutfalla, G., and Mogensen, K. E. (1995) Alpha and beta interferons and their receptor and their friends and relations, *J. Interferon Cytokine Res. 15*, 3−26.
41. Schmeisser, H., Hu, R., Kontsek, P., Bekisz, J., and Zoon, K. (2002) Amino acid substitutions in loop BC and helix C affect antigenic properties of helix D in hybrid IFN-alpha21a/alpha2c molecules, *J. Interferon Cytokine Res. 22*, 463−472.
42. Gauzzi, M. C., Barbieri, G., Richter, M. F., Uzé, G., Ling, L., Fellous, M., and Pellegrini, S. (1997) The amino-terminal region of Tyk2 sustains the level of interferon alpha receptor 1, a component of the interferon alpha/beta receptor, *Proc. Natl. Acad. Sci. U.S.A. 94*, 11839−11844.
43. Ragimbeau, J., Dondi, E., Alcover, A., Eid, P., Uzé, G., and Pellegrini, S. (2003) The tyrosine kinase Tyk2 controls IFNAR1 cell surface expression, *EMBO J. 22*, 537−547.
44. Takaoka, A., Mitani, Y., Suemori, H., Sato, M., Yokochi, T., Noguchi, S., Tanaka, N., and Taniguchi, T. (2000) Cross talk between interferon-gamma and -alpha/beta signaling components in caveolar membrane domains, *Science 288*, 2357−2360.
45. Domanski, P., Nadeau, O. W., Platanias, L. C., Fish, E., Kellum, M., Pitha, P., and Colamonici, O. R. (1998) Differential use of the beta(L) subunit of the type I interferon (IFN) receptor determines signaling specificity for IFN alpha 2 and IFN beta, *J. Biol. Chem. 273*, 3144−3147.
46. Briscoe, J., Rogers, N. C., Witthuhn, B. A., Watling, D., Harpur, A. G., Wilks, A. F., Stark, G. R., Ihle, J. N., and Kerr, I. M. (1996) Kinase-negative mutants of JAK1 can sustain interferon-gamma-inducible gene expression but not an antiviral state, *EMBO J. 15*, 799−809.
47. Mogensen, K. E., Lewerenz, M., Reboul, J., Lutfalla, G., and Uzé, G. (1999) The type I interferon receptor: structure, function, and evolution of a family business, *J. Interferon Cytokine Res. 19*, 1069−1098.
48. Uddin, S., Yenush, L., Sun, X. J., Sweet, M. E., White, M. F., and Platanias, L. C. (1995) Interferon-alpha engages the insulin receptor substrate-1 to associate with the phosphatidylinositol 3′-kinase, *J. Biol. Chem. 270*, 15938−15941.
49. Uddin, S., Fish, E. N., Sher, D. A., Gardziola, C., White, M. F., and Platanias, L. C. (1997) Activation of the phosphatidylinositol 3-kinase serine kinase by IFN-alpha, *J. Immunol. 158*, 2390−2397.
50. Ahmad, S., Alsayed, Y. M., Druker, B. J., and Platanias, L. C. (1997) The type I interferon receptor mediates tyrosine phosphorylation of the CrkL adaptor protein. *J. Biol. Chem. 272*, 29991−29994.
51. David, M., Petricoin, E., 3rd, Benjamin, C., Pine, R., Weber, M. J., and Larner, A. C. (1995) Requirement for MAP kinase (ERK2) activity in interferon alpha- and interferon beta-stimulated gene expression through STAT proteins, *Science 269*, 1721−1723.
52. Goh, K. C., Haque, S. J., and Williams, B. R. (1999) p38 MAP kinase is required for STAT1 serine phosphorylation and transcriptional activation induced by interferons, *EMBO J. 18*, 5601−5608.
53. Li, Y., Sassano, A., Majchrzak, B., Deb, D. K., Levy, D. E., Gaestel, M., Nebreda, A. R., Fish, E. N., and Platanias, L. C. (2004) Role of p38alpha Map kinase in Type I interferon signaling, *J. Biol. Chem. 279*, 970−979.
54. Goldman, L. A., Cutrone, E. C., Dang, A. J., Hao, X. M., Lim, J. K., and Langer, J. A. (1998) Mapping human interferon-alpha (IFN-alpha 2) binding determinants of the type I interferon receptor subunit IFNAR-1 with human/bovine IFNAR-1 chimeras, *Biochemistry 37*, 13003−13010.
55. Krause, C. D., Mei, E., Xie, J., Jia, Y., Bopp, M. A., Hochstrasser, R. M., and Pestka, S. (2002) Seeing the Light: Preassembly and Ligand-Induced Changes of the Interferon gamma Receptor Complex in Cells, *Mol. Cell. Proteomics 1*, 805−815.

56. Pfeffer, L. M., Dinarello, C. A., Herberman, R. B., Williams, B. R. G., Borden, E. C., Bordens, R., Walter, M. R., Nagabhushan, T. L., Trotta, P. P., and Pestka, S. (1998) Biological properties of recombinant alpha-interferons: 40th anniversary of the discovery of interferons, *Cancer Res. 58*, 2489−2499.
57. Zoon, K. C., Miller, D., Bekisz, J., zur Nedden, D., Enterline, J. C., Nguyen, N. Y., and Hu, R. Q. (1992) Purification and characterization of multiple components of human lymphoblastoid interferon-alpha, *J. Biol. Chem. 267*, 15210−15216.
58. Yanai, Y., Sanou, O., Kayano, T., Ariyasu, H., Yamamoto, K., Yamauchi, H., Ikegami, H., and Kurimoto, M. (2001) Analysis of the antiviral activities of natural IFN-alpha preparations and their subtype compositions, *J. Interferon Cytokine Res. 21*, 835−841.
59. Hu, R., Gan, Y., Liu, J., Miller, D., and Zoon, K. C. (1993) Evidence for multiple binding sites for several components of human lymphoblastoid interferon-alpha, *J. Biol. Chem. 268*, 12591−12595.
60. Hu, R., Bekisz, J., Hayes, M., Audet, S., Beeler, J., Petricoin, E., and Zoon, K. (1999) Divergence of binding, signaling, and biological responses to recombinant human hybrid IFN, *J. Immunol. 163*, 854−860.
61. Karpusas, M., Nolte, M., Benton, C. B., Meier, W., Lipscomb, W. N., and Goelz, S. (1997) The crystal structure of human interferon beta at 2.2-angstrom resolution, *Proc. Natl. Acad. Sci. U.S.A. 94*, 11813−11818.

BI049111R